Zitierweise: *Angew. Chem. Int. Ed.* **2024**, *63*, e202405750
doi.org/10.1002/anie.202405750

Chloride-Ion Batteries

Design of Solid Polycationic Electrolyte to Enable Durable Chloride-Ion Batteries

Xu Yang, Zhiqiang Fu, Ran Han, Yaojie Lei, Shijian Wang, Xin Zhao, Yuefeng Meng, Hao Liu, Dong Zhou, Doron Aurbach,* and Guoxiu Wang**

Abstract: The high energy density and cost-effectiveness of chloride-ion batteries (CIBs) make them promising alternatives to lithium-ion batteries. However, the development of CIBs is greatly restricted by the lack of compatible electrolytes to support cost-effective anodes. Herein, we present a rationally designed solid polycationic electrolyte (SPE) to enable room-temperature chloride-ion batteries utilizing aluminum (Al) metal as an anode. This SPE endows the CIB configuration with improved air stability and safety (i.e. free of flammability and liquid leakage). A high ionic conductivity (1.3×10^{-2} S cm^{-1} at 25 °C) has been achieved by the well-tailored coordination structure of the SPE. Meanwhile, the solid polycationic electrolyte ensures stable electrodes|electrolyte interfaces, which effectively inhibit the growth of dendrites on the Al anodes and degradation of the FeOCl cathodes. The Al|SPE|FeOCl chloride-ion batteries showcased a high discharge capacity around 250 mAh g^{-1} (based on the cathodes) and extended lifespan. Our electrolyte design opens a new avenue for developing low-cost chloride-ion batteries.

Introduction

Lithium (Li)-ion batteries have been widely used in consumer electronics, electric vehicles, and energy storage applications. However, the limited reserves and uneven distribution of their core constituent elements (e.g. Li and cobalt) lead to the high cost for Li-ion batteries and their limited potential use for large-scale energy storage.[1] Therefore, developing low-cost alternative battery systems is urgently needed to meet the ever-growing market demands. Chloride-ion batteries are a new type of rechargeable battery system employing chloride ions (Cl^-) as the charge carriers, which operate based on a "rocking-chair" chemistry similar to Li-ion batteries but utilizing Cl^- ions shuttling between the electrodes.[2] The application of chlorides storage cathodes (metal chloride,[3] metal oxychloride[4] and layered double hydroxide[5]) and highly electropositive metal anodes endow the CIBs with high theoretical energy densities up to around 1100 Wh kg^{-1} and 2500 Wh L^{-1}.[6] Meanwhile, the abundance of elemental chlorine makes CIBs cost-effective. Moreover, CIBs possess the advantages of lower toxicity and higher environmental safety over fluoride-ion batteries, thus benefiting from practical applicability for electrochemical energy storage.[7] However, the development of CIBs is still in its infancy owing to the lack of compatible electrolytes. Most previous reported electrolytes of CIBs only allow highly reactive Li metal as anode, which nevertheless has a high cost and is extremely sensitive to air and humidity.[8] Some ionic liquid electrolytes (ILEs) have also been employed in CIBs to enable the magnesium (Mg) metal anodes, but their poor anode|electrolyte compatibility results in low reversibility and limited cycle life.[9] Therefore, designing new electrolyte to support low-cost and compatible anode materials remains a major bottleneck for the development of CIBs.

Compared to Li and Mg, aluminum (Al) possesses low cost merit due to its abundance and wide distribution in the earth's crust.[10] Furthermore, with the relatively low potential (−1.66 V vs. SHE) and high volumetric capacity (i.e. 8.04 Ah cm^{-3}, four times higher than that of Li), Al metal is an ideal choice as anode materials for low-cost battery systems.[10] Pairing Al metal anode with a transition metal oxychloride cathode is a promising path to construct high-performance and low-cost CIBs. However, to the best of our knowledge, such systems has not yet been previously reported. The main challenge lies in the lack of suitable electrolyte systems to support the redox pair in Al-based CIBs.[11] In the 1970s, high-temperature chloroaluminate

[*] X. Yang, Y. Lei, S. Wang, H. Liu, G. Wang
Centre for Clean Energy Technology
Faculty of Science
University of Technology Sydney
Sydney, NSW 2007, Australia
E-mail: guoxiu.wang@uts.edu.au

Z. Fu, R. Han, X. Zhao, Y. Meng, D. Zhou
Tsinghua Shenzhen International Graduate School
Tsinghua University
Shenzhen 518055, P. R. China
E-mail: zhou.d@sz.tsinghua.edu.cn

D. Aurbach
Department of Chemistry and Bar-Ilan Institute of Nanotechnology and Advanced Materials
Bar-Ilan University
Ramat-Gan 5290002, Israel
E-mail: doron.aurbach@biu.ac.il

molten salt electrolytes (e.g. NaCl-$AlCl_3$) were applied in rechargeable Al metal batteries.[12] Then the emergence of room-temperature chloroaluminate ILEs enabled a reversible Al plating/stripping under more practical conditions.[13] Among them, an $AlCl_3$/1-ethyl-3-methylimidazolium chloride ([EMIM]Cl) mixture at the optimized molar ratio of 1.3:1 with high room-temperature ionic conductivity up to 10^{-2} S cm^{-1} has been widely used in rechargeable Al-based batteries.[14] Nonetheless, the intrinsic drawbacks of this pure liquid ILE system, including high air sensitivity,[15] corrosivity,[16] liquid leakage issues, and interfacial issues (e.g. Al dendritic growth,[1b] low Al plating/stripping reversibility,[1b] together with poor compatibility with relevant cathodes such FeOCl), present an enormous challenge to the development of Al-based CIBs (see upper panel of Figure 1a).

Herein, for the first time, we report a rationally designed solid polycationic electrolyte (SPE) to realize the application of Al metal anode in a room-temperature CIB. This SPE derived from the in situ polymerization of 1-allyl-3-methylimidazolium cations ($[AMIM]^+$) in $AlCl_3$/[AMIM]Cl precursor was rationally designed for this Al-based CIB. Compared to previous ILEs, this SPE exhibits enhanced air stability, non-flammability, and leakage-free endurance (lower panel of Figure 1a). More importantly, both computational modeling and spectroscopic investigations reveal that the tailored coordination structure in the SPE not only efficiently promotes ions conduction (i.e. ionic conductivity of 1.4×10^{-2} S cm^{-1} at 25 °C) and increases the anion transference number of the charge carriers, but also maintains stable electrode|electrolyte interfaces against Al dendritic growth on the anode and FeOCl cathodes degradation, thereby dramatically enhancing the reversibility of both electrodes' reactions. By virtue of the SPE, the as-developed Al||FeOCl CIB could deliver a high discharge capacity around 250 mAh g^{-1} (based on the cathode) with extended cyclability. This work provides a promising route for the development of highly energetic, durable, and low-cost CIBs.

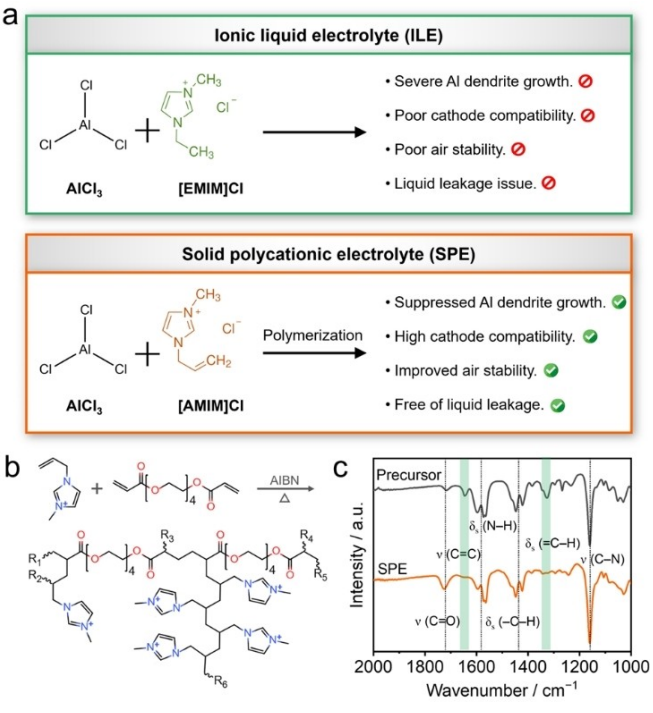

Figure 1. Design and synthesis of the SPE. (a) Design philosophy of the SPE for Al-based CIBs. (b) Co-polymerization mechanism of the $[AMIM]^+$ monomer and the TEGDA crosslinker. R_i (i = 1–6) represents molecular chains. (c) FTIR spectra of precursor and SPE.

Results and Discussion

To synthesize the SPE, a precursor was prepared by mixing $AlCl_3$ and [AMIM]Cl at a molar ratio of 1.25:1, followed by the adding of tetra(ethylene glycol) diacrylate (TEGDA) crosslinker, based on the reaction as follows:[11,14]

$$Cl^- + AlCl_3 \leftrightarrow AlCl_4^- \quad (1)$$

$$2AlCl_4^- \leftrightarrow Cl^- + Al_2Cl_7^- \quad (2)$$

After that, $[AMIM]^+$ cation monomers and the crosslinkers in the precursor were thermally co-polymerized by the cross-linking reaction initiated by the azobisisobutyronitrile (AIBN) to form the SPE (Figure 1b). Figure 1c shows the Fourier transform infrared (FTIR) spectra of the precursor and the SPE. It is seen that absorption peaks at around 1723 cm^{-1} (C=O stretching), 1582 cm^{-1} (N–H symmetric bending), 1439 cm^{-1} (–C–H symmetric bending) and 1163 (C–N stretching) appeared in the spectrum of the precursor.[17] After the polymerization, the C=C stretching peak at around 1646 cm^{-1} and =C–H symmetric bending peak at around 1439 cm^{-1} almost vanished, indicating the conversion of $[AMIM]^+$ and TEGDA in the SPE.

As shown in Figure 2a, in contrast to the fluidic $AlCl_3$/[EMIM]Cl ILE (1.25:1 in molar ratio), the as-synthesized SPE is brown translucent, and free-standing. Furthermore, the SPE exhibits a zero self-extinguishing time (SET) after removal of a flammability test torch (Figure 2b and Video S1), demonstrating its intrinsic nonflammability originating from the high thermal stability of the aromatic imidazole ring on the polymerized $[AMIM]^+$ and the generation of antioxidants during thermal decomposition.[18] This result was further verified by the differential scanning calorimetry (DSC). As shown in Figure S1, the endothermic peak observed at 100 °C is attributed to the melting phase transition of chloroaluminate in the SPE.[19] No additional peaks emerge up to 500 °C, indicating the thermal stability of the SPE. Figure 2c shows a leakage test being performed, where the packages containing electrolytes were cut and weighted after pressing and hanging. The ILE package exhibited a 74 wt % leakage during the test, while the SPE was nearly leak-free (i.e. only 5 wt % weight loss; Figure 2d). Subsequently, the packages were hung for a further 5 min. Moreover, it is known that the chloride species in chloroaluminate electrolytes have a strong affinity to water. When exposed to air, the high hygroscopic chloroaluminate

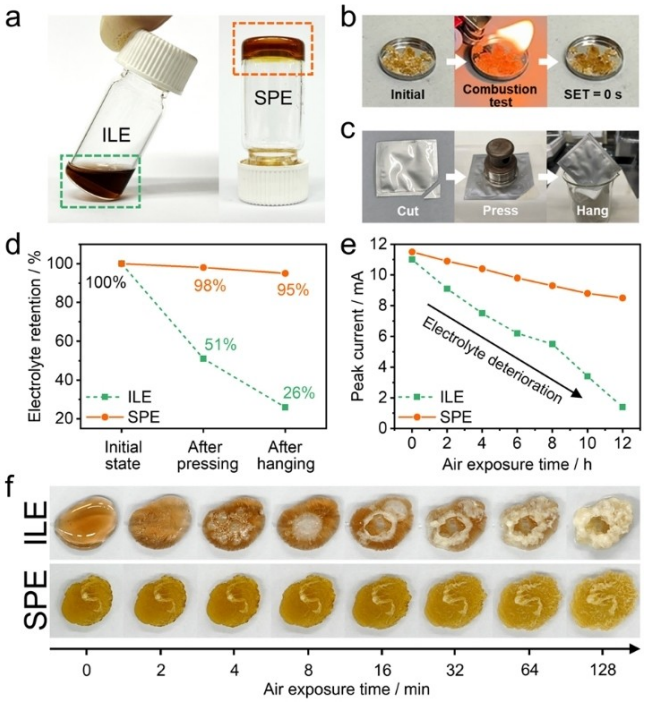

Figure 2. Safety of SPE. Optical images of (a) liquid-state ILE (left) and solid-state SPE (right), and (b) SPE during combustion tests. (c) Visual observation of electrolyte samples under different leakage test states. (d) Weight retentions of ILE and SPE during leakage tests. (e) Peak current evolution of Al||Al cells with ILE and SPE under air exposure. (f) Optical images of ILE and SPE during air exposure.

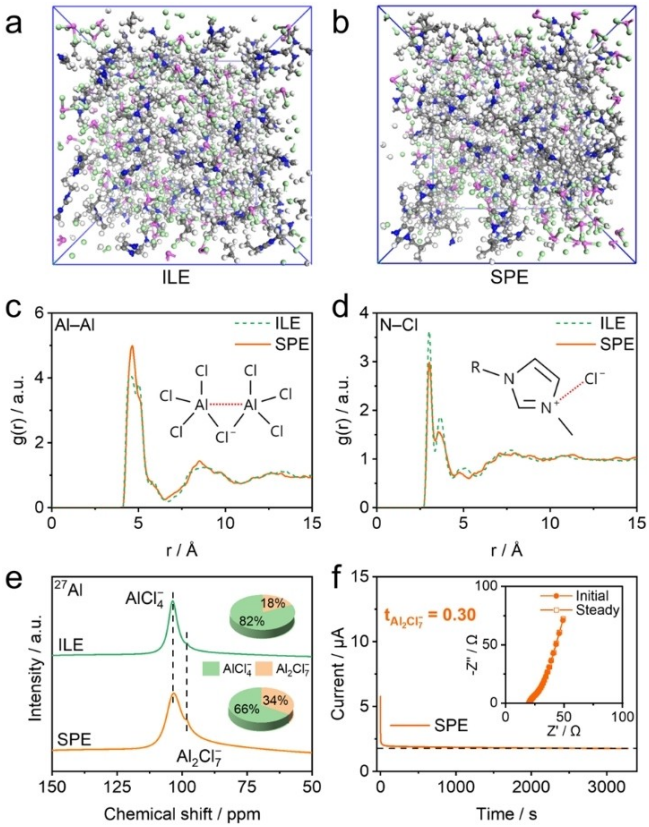

Figure 3. Coordination structure in the SPE. Snapshots obtained from MD simulations of (a) ILE and (b) SPE. Purple, green, gray, white, and blue balls represent aluminum, chlorine, carbon, hydrogen, and nitrogen atoms, respectively. MD simulations derived RDFs of (c) Al–Al coordination pairs and (d) N–Cl coordination pairs. Insets show the molecular schematics of coordination pairs. (e) Al^{27} NMR spectra of ILE and SPE. Insets show the ratios of $AlCl_4^-$ and $Al_2Cl_7^-$ species. (f) Current passes through Al|SPE|Al cells with an applied polarization voltage of 10 mV. The impedance spectra before and after the polarization are shown in the inset. Related parameters are listed in Table S1.

electrolytes violently react with moisture, generating a huge amount of heat and releasing undesirable and corrosive hydrogen chloride gas,[14,20] which raises serious safety concerns. The as-prepared SPE with high-crosslink-density polycation-crosslinker network effectively blocks moisture diffusion, and thus inhibits its continuous reaction with chloroaluminate. As shown in Figure 2e, the peak current derived from cyclic voltammetry (CV) curves of an Al|ILE|Al cell (Figure S2) exhibits a dramatic decrease throughout air exposure. This is further reflected by the optical images in the upper panel of Figure 2f, in which the hygroscopic ILE can be seen to decompose rapidly during air exposure. In sharp contrast, the SPE showed enhanced resistance against moisture (the lower panel of Figure 2f) and the peak current of Al|SPE|Al cells delivered a remarkably improved stability after exposure to air (Figure 2e). The above results indicate that the SPE can efficiently prevent the CIBs from combustion and leakage of corrosive liquid/gas components, thus improving the safety of Al-based CIBs.

Molecular dynamics (MD) simulation was employed to investigate the coordination structures of chloroaluminate ions (i.e. $AlCl_4^-$ and $Al_2Cl_7^-$) and alkylimidazolium cations (i.e. $[EMIM]^+$ or $[AMIM]^+$). The snapshots at the end of the simulations demonstrate the steady coordination environments of ILE (Figure 3a) and SPE (Figure 3b). As seen from the corresponding radial distribution function (RDF) of Al–Al coordination pairs (Figure 3c), the peak at 4.62 Å in the SPE is stronger than that in ILE, indicating the higher concentration of the $Al_2Cl_7^-$ species in SPE.[21] Moreover, it is seen that the RDF of N–Cl displayed two peaks at 3.02 Å and 3.65 Å, and their intensities in the SPE are much weaker than that in ILE (Figure 3d). This indicates that the dissociation degree of alkylimidazolium chloride is effectively promoted in the SPE, which can be further verified by the spectral characterizations. As shown in the Al^{27} nuclear magnetic resonance (NMR) spectra (Figure 3e), the area ratio between $Al_2Cl_7^-$ (98.3 ppm) and $AlCl_4^-$ (103.6 ppm) peaks[22] in the SPE is 0.51, much higher than that in ILE (i.e. 0.27). The Raman spectral results in Figure S3 are well consistent with this result, where the $Al_2Cl_7^-$ vibration peaks in the SPE spectrum are stronger than that in the ILE spectrum.

The $Al_2Cl_7^-$-rich coordination structure and high salt dissociation degree of SPE mainly originate from the polymerization of cations that effectively confines their mobility and promotes the decoupling from anions.[23] Thereby, the SPE exhibited a high anion transference

number of 0.30 (Figure 3f and Table S1) measured by Bruce-Vincent method,[24] almost twice than that in the ILE (0.16, Figure S4 and Table S1). Based on a modified Hittorf method as reported by Chester et al.,[25] the anions transport number of SPE was determined as 0.25, greater than that of ILE (0.14). This trend is consistent with the transference number result. The increase of anion transference/transport number for charge carriers can efficiently reduce battery polarization, resulting in more uniform Al electrodeposition with high Coulombic efficiency.[15] As expected, the SPE exhibits a high ionic conductivity (1.3×10^{-2} S cm^{-1} at 25 °C) after polymerization (Figure S5 and Table S2), nearly the same as that of ILE (1.5×10^{-2} S cm^{-1} at 25 °C) due to the tailored coordination structure with increased degree of salt dissociation. The SPE also exhibited higher oxidation stability (2.6 V vs. Al^+/Al) than that of ILE (Figure S6). Such high ionic conductivity and electrochemical stability of SPE are sufficient for room-temperature operation of the Al-based CIBs.

Al||Al Swagelok cells were assembled to evaluate the compatibility of the Al metal anode|electrolyte interfaces. Figure 4a shows the CV curves of an Al|SPE|Al cell at a scan rate of 0.5 mV s^{-1}. The highly symmetrical redox peak pairs at around ±0.3 V indicate a reversible Al plating/stripping reaction as follows:[11]

$$\text{Anode}: Al + 7AlCl_4^- \leftrightarrow 4Al_2Cl_7^- + 3e^- \quad (3)$$

The highly overlapping CV curves after the initial cycles verify the stable electrochemical stripping/depositing processes of Al metal in the SPE. As shown in Figure 4b, the high compatibility between SPE and Al metal enabled the Al|SPE|Al cell to operate steadily at a high current density of up to 5 mA cm^{-1} with a capacity cutoff of 1 mAh cm^{-1}.

Moreover, the overpotential between the voltages of the Al|SPE|Al symmetrical cell remained stable for the 2000 h cycling at 1 mA cm^{-2} with a cut-off capacity of 1 mAh cm^{-2} (Figure 4c). In contrast, the voltage hysteresis of the Al|ILE|Al cell gradually increased after 125 cycles and short-circuited after ≈500 cycles caused by Al dendrites growth. The surface structure of Al electrodes after 100 cycles in Al||Al cells was further characterized by an atomic force microscope (AFM). As can be seen in the three-dimensional (3D) scanning image in the inset of Figure 4d, the surface of Al electrodes cycled in SPE showed a smooth morphology with a low roughness of 85.2 nm. This validates a dense and uneven deposition of Al metal, as further confirmed by the scanning electron microscope (SEM) image (Figure 4e) and a high Young's modulus of the Al surface (17.8 GPa, Figure 4d). In sharp contrast, the Al electrodes cycled in ILE exhibited a high roughness of 90.4 nm (see Figure S7, inset) with a low Young's modulus (12.6 GPa, Figure S7) and porous morphology (Figure 4d, inset) due to the uncontrollable growth of Al dendrites, which is in good agreement with the cycling performance results in Figure 4c.

To examine the performance of SPE in Al-based CIBs, a FeOCl cathode with a mass loading of ≈1.0 mg cm^{-2} was coupled with an Al metal anode in Swagelok cells. Figure S8 shows typical CV curves of Al|SPE|FeOCl cells under a scan rate of 0.2 mV s^{-1} at 25 °C. Three oxidation peaks at around 0.58, 0.66, and 0.76 V together with two corresponding broad reduction peaks at around 0.2 and 0.4 V appear in the CV curves. These redox peaks are consistent with the multistep electrochemical chlorination/de-chlorination behavior of FeOCl materials.[26] Therefore, the Cl-ion discharge/charge process of FeOCl cathode with SPE can be expressed as follows: follows:[27]

$$\text{Cathode}: FeOCl + Al_2Cl_7^- + e^- \leftrightarrow FeO + 2AlCl_4^- \quad (4)$$

Considering that the Cl^- ion in cathode and $AlCl_3$ as discharge product can reversibly convert into chloroaluminate ions (i.e. $AlCl_4^-$ and $Al_2Cl_7^-$) based on Equation 1 and 2. Therefore, Cl^- ions can be regarded as the actual charge carriers shuttling between the anode and cathode based on a rocking chair mechanism. Based on the above discussion, we define this battery system as a chloride-ion battery. The overall reaction of this Al-based CIB can be expressed as follows:

$$Al + 3FeOCl + AlCl_4^- \leftrightarrow 3FeO + Al_2Cl_7^- \quad (5)$$

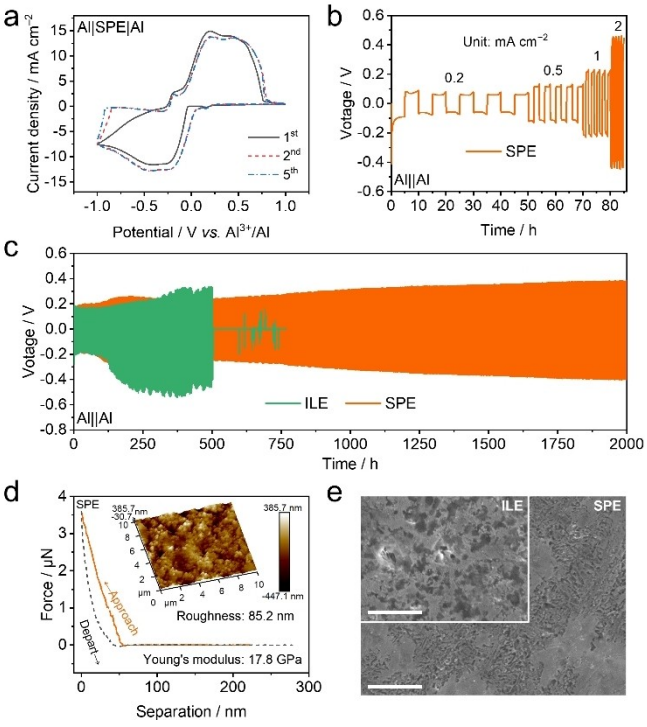

Figure 4. Interfacial compatibility between SPE and Al metal anodes. (a) CV curves of the Al|SPE|Al cell at a scan rate of 0.5 mV s^{-1}. (b) Rate performance of a typical Al|SPE|Al cell at 25 °C. (c) Voltage profiles of Al||Al cells with ILE and SPE at 1 mA cm^{-2} with a cut-off capacity of 1 mAh cm^{-2}. (d) Force-displacement plot of the Al surface obtained from an Al|SPE|Al cell after 100 cycles. The inset shows the corresponding 3D AFM scanning image. (e) SEM images of Al surfaces obtained from Al||Al cells after 100 cycles with ILE (inset) and SPE. Scale bars: 5 μm in Figure 4e and its inset.

Figures 5a and b show the cycling performance of Al||FeOCl cells with different electrolytes galvanostatically cycled at 125 mA g^{-1} (based on the mass of FeOCl) at 25 °C. After initial activation cycles, the Al|ILE|FeOCl cells exhibited a low discharge capacity around 54 mAh g^{-1} (based on the mass of FeOCl) at the 2nd cycle (Figure 5a), and subsequently failed within 10 cycles caused by the poor compatibility of the ILE and the electrodes (Figure 5b). In contrast, the Al|SPE|FeOCl cells delivered a discharge capacity of approaching 250 mAh g^{-1} (based on the mass of FeOCl) after activation with lower polarization and high Coulombic efficiency (CE), achieving a high capacity retention of 85.4 % after 120 cycles (Figures 5a,b). The above results are further supported by the resistance evolution derived from the Nyquist plots of electrochemical impedance spectroscopy (EIS) measurements for the Al||FeOCl cells with different electrolytes after 2 and 5 cycles (Figure S9 and Table S3). The EIS curves were fitted using an equivalent circuit demonstrated in the inset of Figure 5c. Based on the fitting result, the charge-transfer resistance (R_{ct}) and the interface resistance (R_f) of the Al||FeOCl cells using SPE underwent much smaller variations during cycling compared with that using ILE (Figure 5c). This suggests a strong interfacial stability between the SPE and the electrodes, thereby giving rise to the enhanced cycling performance (Figures 5b). Figure 5d and Table S4 compared the performance of the Al-based CIB presented in this study with the previously reported non-Li metal CIBs[9] and Al-ion batteries (AIBs).[28] Our Al||FeOCl CIB supported by SPE exhibited an obvious superiority in terms of high discharge capacity, long cycle life, high CE, and good rate performance (discharge capacities of 108 and 43 mAh g^{-1} at 250 at 500 mA g^{-1}, respectively; Figure S10), outperforming most low-cost non-Li metal CIBs and AIBs.

Besides, our SPE showed high versatility for extension into Al metal||graphite AIB systems. The CV curves of an Al|SPE|graphite cell in Figure S11 are consistent with previous reports based on a reaction mechanism as follows:[11,29]

$$Al + 3C_n[AlCl_4] + 4AlCl_4^- \leftrightarrow 3C_n + 4Al_2Cl_7^- \quad (6)$$

Al|SPE|graphite test cells delivered a stable discharge capacity of ≈31 mAh g^{-1} at 1.5 mA g^{-1}, and ≈88 mAh g^{-1} at 0.3 mA g^{-1} with discharge plateaus at 2.2 and 1.8 V (inset of Figure 5e). After 1000 cycles, the cell maintained a discharge capacity of 81 mAh g^{-1} (i.e. 92.0 % capacity retention) with an average CE of 99.2 % (Figure 5e), demonstrating the application merits of the SPE developed in the present study in low-cost and durable Al-based rechargeable battery systems.

The compatibility of anode|electrolyte interphase in the full cell was evaluated by SEM and dispersive X-ray spectroscopy (EDS). As shown in Figure S12, a thick and cracked solid electrolyte interphase (SEI) with weak Al signal and strong organic species signals was observed on Al anode from Al|ILE|FeOCl cell. In contrast, the SEI on Al metal with SPE is flat and thin, as verified by the intense Al signal with uniform organic species signals (Figure S13). These results indicate that the polycation-structured SPE efficiently protects the Al anode by building robust SEI aqainst the continuous electrolyte decomposition.

In situ analysis of synchrotron powder diffraction (PD) was applied to investigate the structural evolution of the FeOCl cathode during discharging /charging. The peaks at 26.10°, 41.58°, and 50.47° can be attributed to (110), (130) and (131) planes of FeOCl (PDF#73-2229), respectively, while the peak at 41.89° corresponds to the (200) planes of FeO (PDF#77-2355; Figure 6a). During the discharge process, the intensity of FeOCl-related peaks is gradually weakened, associated with the intensity increase of the FeO peak, then an opposite trend of peaks' evolution was observed during the subsequent charging process. This verifies the high reversibility of FeOCl in the presence of the SPE developed herein, which can be further confirmed by Fe 2*p* and O 1*s* X-ray photoelectron spectra (XPS). The Fe $2p_{3/2}$ peak at 710.5 eV (Figure 6b) and the O 1*s* peak at 531.4 eV (Figure S14) are assigned to the FeOCl.[2a] It is seen that FeO peaks (Fe $2p_{3/2}$ at 708.2 eV and O 1*s* at 529.5 eV)[2a] emerged and then vanished during the discharge/re-charging process, well supporting the suggested

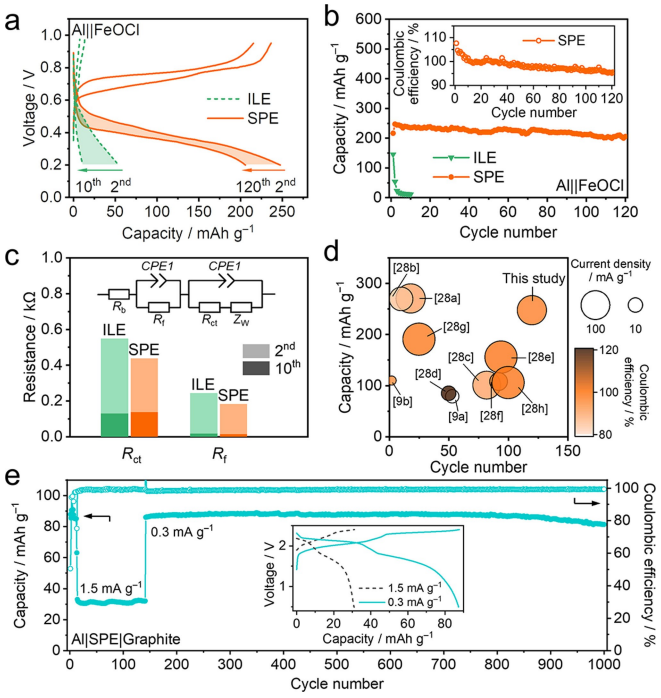

Figure 5. Electrochemical performance of the Al-based CIBs. (a) Typical galvanostatic discharge/charge profiles and (b) cycling performance of Al||FeOCl cells with ILE and SPE at 125 mA g^{-1} and 25 °C. The inset in Figure 5b shows the CE of an Al|SPE|FeOCl cell. (c) Resistance evolution was obtained from the EIS measurement for Al||FeOCl cells with ILE and SPE after 2 and 10 cycles. The inset shows the equivalent circuit analogue for the EIS curves' fitting. Related parameters are listed in Table S3. (d) Performance comparison of the reported non-Li metal CIBs[9] and Al-ion AIBs[28] and the Al|SPE|FeOCl cells developed in this study. Related parameters are listed in Table S4. (e) Cycling performance and typical galvanostatic discharge/charge profiles (inset) of a typical Al|SPE|graphite cell at 25 °C.

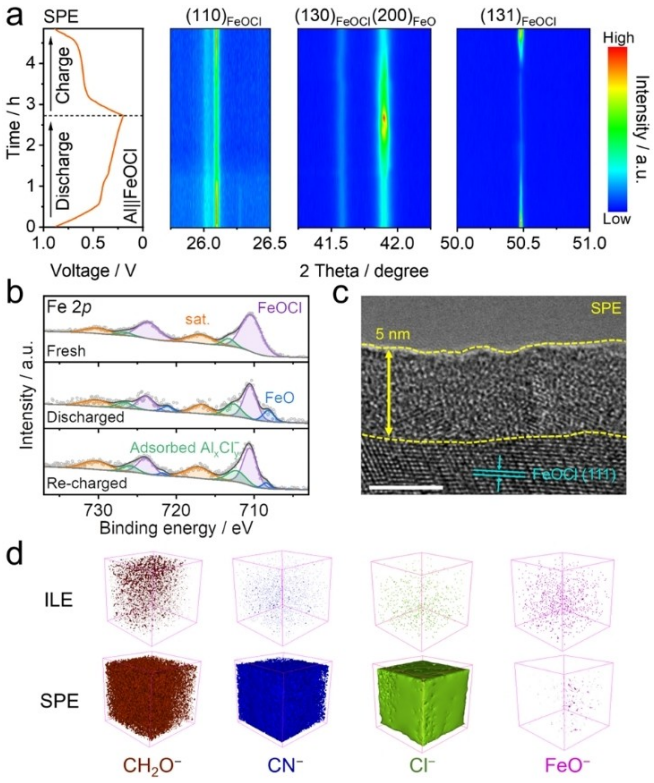

Figure 6. Characterizations of cycled FeOCl cathodes. (a) In situ synchrotron powder diffraction (PD) analysis of the structural evolution of FeOCl cathodes during discharge/charge processes. Left panel presents the voltage profile of the Al | SPE | FeOCl cell, while the right panel shows the corresponding intensity map of the PD pattern for a FeOCl cathode, where red and blue indicate high and low intensity, respectively. (b) Fe 2*p* XPS peaks of FeOCl electrodes cycled in SPE at fresh, fully discharged, and fully re-charged states. (c) A TEM image of a FeOCl electrode obtained from an Al | SPE | FeOCl cell after 3 cycles at 125 mA g^{-1} and 25 °C. Scale bar: 4 nm. (d) 3D-geometric structures of the TOF-SIMS intensity distributions related to CH_2O^- (brown), CN^- (blue), Cl^- (green), and FeO^- (pink) for FeOCl electrodes obtained from cycled Al | | FeOCl cells with ILE (upper panel) and SPE (lower panel) after 3 cycles at 125 mA g^{-1} and 25 °C.

reversible reaction mechanism of FeOCl described in Equation 4.

The compatibility of the SPE and the cathode was further investigated to understand the origin of the high performance of the FeOCl cathodes with the SPE. FeOCl cathodes after cycling in different electrolytes were analyzed by transmission electron microscopy (TEM). As seen in Figure S15, a cracked FeOCl structure was observed for FeOCl cathodes cycled in cells containing ILE. This is caused by the continuous dissolution of Fe cations from the exposed FeOCl surface, as confirmed by the element analysis of cycled cathode in Table S5, which leads to a rapid structure degeneration and cyclability fading of the cathode.[2a] In contrast, a 5 nm-thick protective surface film was formed on the FeOCl surface after cycling in SPE (Figure 6c). This result was further proved by time-of-flight secondary ion mass spectrometry (ToF-SIMS) with high resolution (<1 nm). In contrast to FeOCl cycled in ILE (upper panel of Figure 6d), the cathode cycled in SPE presented an organic species-rich film on the surface, as supported by the detection of highly intense signals of CH_2O^- and CN^- (lower panel of Figure 6d). This protective surface film can effectively maintain the structural integrity of FeOCl against dissolution/degeneration during cycling (as seen from clear lattice fringes of FeOCl (110) planes in Figure 6c), thus remarkably extending the cycling performance of the FeOCl cathodes.

Conclusion

In summary, we have showcased a rationally designed solid polycationic electrolyte that enables elaboration of novel room-temperature chloride-ion batteries employing cost-effective Al metal anodes. The solid polycationic electrolyte derived from the in situ polymerization of $[AMIM]^+$ cations efficiently eliminates the hazards of air sensitivity and liquid leakage encountered with conventional electrolyte systems based on ionic liquids or non-aqueous solutions. Molecular dynamics modeling and experimental characterizations emphasize the tailored coordination structure within the solid polycationic electrolyte, which not only improves the ions conduction (1.3×10^{-2} S cm^{-1} at 25 °C) and the charge carrier's anion transference number, but also forms compatible interfaces between the electrodes and the SPE to effectively avoid electrodes' deterioration (i.e., impeding Al dendritic deposition on the anode and FeOCl degradation at the cathode side) along cycling. Therefore, the as-developed Al | SPE | FeOCl chloride-ion batteries deliver high discharge capacity and appealing cycling stability. The Al-based chloride-ion batteries could be potentially applied for grid-scale energy storage owing to their low cost, high-energy density, long cycle life and abundant of materials.

Supporting Information

The authors have cited additional references within the Supporting Information.

Acknowledgements

Prof. G. Wang would like to acknowledge the support from the Australian Research Council (ARC) Discovery Project (DP210101389 and DP230101579) and the ARC Linkage project (LP200200926). Prof. D. Zhou would like to acknowledge the support from the Fundamental Research Project of Shenzhen (NO. JCYJ20230807111702005). We like to acknowledge the Australia Synchrotron for the Powder Diffraction beamline. Open Access publishing facilitated by University of Technology Sydney, as part of the Wiley - University of Technology Sydney agreement via the Council of Australian University Librarians.

Conflict of Interest

The authors declare no conflict of interest.

Keywords: chloride-ion battery · solid polycationic electrolyte · aluminum metal anode · air stability · interfacial compatibility

[1] a) Y. Meng, D. Zhou, R. Liu, Y. Tian, Y. Gao, Y. Wang, B. Sun, F. Kang, M. Armand, B. Li, G. Wang, D. Aurbach, *Nat. Energy* **2023**, *8*, 1023; b) Z. Zhang, X. Yang, P. Li, Y. Wang, X. Zhao, J. Safaei, H. Tian, D. Zhou, B. Li, F. Kang, G. Wang, *Adv. Mater.* **2022**, *34*, e2206970.
[2] a) X. Yang, B. Zhang, Y. Tian, Y. Wang, Z. Fu, D. Zhou, H. Liu, F. Kang, B. Li, C. Wang, G. Wang, *Nat. Commun.* **2023**, *14*, 925; b) Z. Xue, Z. Gao, X. Zhao, *Energy Environ. Mater.* **2022**, *5*, 1155; c) X. Zhao, Z. Zhao-Karger, M. Fichtner, X. Shen, *Angew. Chem. Int. Ed.* **2020**, *59*, 5902.
[3] T. Xia, Q. Li, X. Zhao, X. Shen, *Adv. Mater.* **2024**, *36*, e2310565.
[4] a) P. Gao, M. A. Reddy, X. Mu, T. Diemant, L. Zhang, Z. Zhao-Karger, V. S. Chakravadhanula, O. Clemens, R. J. Behm, M. Fichtner, *Angew. Chem. Int. Ed.* **2016**, *55*, 4285; b) X. Zhao, Z. Zhao-Karger, D. Wang, M. Fichtner, *Angew. Chem. Int. Ed.* **2013**, *52*, 13621.
[5] a) Q. Yin, J. Luo, J. Zhang, S. Zhang, J. Han, Y. Lin, J. Zhou, L. Zheng, M. Wei, *Adv. Funct. Mater.* **2019**, *30*, 1907448; b) Q. Yin, D. Rao, G. Zhang, Y. Zhao, J. Han, K. Lin, L. Zheng, J. Zhang, J. Zhou, M. Wei, *Adv. Funct. Mater.* **2019**, *29*, 1900983.
[6] a) X. Zhao, S. Ren, M. Bruns, M. Fichtner, *J. Power Sources* **2014**, *245*, 706; b) J. Yang, Y. Liu, Y. Zhang, G. Wang, X. Shi, H. Zhang, J. Li, P. Deng, X. Tian, *Nano Energy* **2023**, *110*, 108364.
[7] Q. Liu, Y. Wang, X. Yang, D. Zhou, X. Wang, P. Jaumaux, F. Kang, B. Li, X. Ji, G. Wang, *Chem* **2021**, *7*, 1993.
[8] X. Wu, G. Ji, J. Wang, G. Zhou, Z. Liang, *Adv. Mater.* **2023**, *35*, e2301540.
[9] a) P. Gao, X. Zhao, Z. Zhao-Karger, T. Diemant, R. J. Behm, M. Fichtner, *ACS Appl. Mater. Interfaces* **2014**, *6*, 22430; b) X. Zhao, Q. Li, Z. Zhao-Karger, P. Gao, K. Fink, X. Shen, M. Fichtner, *ACS Appl. Mater. Interfaces* **2014**, *6*, 10997.
[10] E. Faegh, B. Ng, D. Hayman, W. E. Mustain, *Nat. Energy* **2020**, *6*, 21.
[11] J. Tu, W. L. Song, H. Lei, Z. Yu, L. L. Chen, M. Wang, S. Jiao, *Chem. Rev.* **2021**, *121*, 4903.
[12] G. L. Holleck, *J. Electrochem. Soc.* **1972**, *119*, 1158.
[13] G. F. Reynolds, C. J. Dymek, *J. Power Sources* **1985**, *15*, 109.
[14] D. Ma, D. Yuan, C. Ponce de León, Z. Jiang, X. Xia, J. Pan, *Energy Environ. Mater.* **2022**, *6*, e12301.
[15] Z. Huang, W. L. Song, Y. Liu, W. Wang, M. Wang, J. Ge, H. Jiao, S. Jiao, *Adv. Mater.* **2022**, *34*, e2104557.
[16] Y. Oh, G. Lee, Y. Tak, *ChemElectroChem* **2018**, *5*, 3348.
[17] X. G. Sun, Y. Fang, X. Jiang, K. Yoshii, T. Tsuda, S. Dai, *Chem. Commun.* **2016**, *52*, 292.
[18] P. Biswas, Y. Wang, E. Hagen, M. R. Zachariah, *J. Am. Chem. Soc.* **2023**, *145*, 16318.
[19] M. Zhang, R. Groves, R. M. Counce, J. S. Watson, T. A. Zawodzinski, *J. Therm. Anal. Calorim.* **2015**, *124*, 395.
[20] K. S. Siefert, *Polyaluminum Chlorides*, Wiley **2000**.
[21] M. Kosar, S. M. Taimoory, O. Diesenhaus, J. F. Trant, *J. Chem. Phys.* **2023**, *159*, 144503.
[22] C. Ferrara, V. Dall'Asta, V. Berbenni, E. Quartarone, P. Mustarelli, *J. Phys. Chem. C.* **2017**, *121*, 26607.
[23] K. M. Abraham, Z. Jiang, B. Carroll, *Chem. Mater.* **1997**, *9*, 1978.
[24] J. Evans, C. A. Vincent, P. G. Bruce, *Polymer* **1987**, *28*, 2324.
[25] C. J. Dymek, L. A. King, *J. Electrochem. Soc.* **2019**, *132*, 1375.
[26] a) X. Zhao, Q. Li, T. Yu, M. Yang, K. Fink, X. Shen, *Sci. Rep.* **2016**, *6*, 19448; b) T. Yu, X. Zhao, L. Ma, X. Shen, *Mater. Res. Bull.* **2017**, *96*, 485; c) T. Yu, R. Yang, X. Zhao, X. Shen, *ChemElectroChem* **2019**, *6*, 1761.
[27] T. Yu, Q. Li, X. Zhao, H. Xia, L. Ma, J. Wang, Y. S. Meng, X. Shen, *ACS Energy Lett.* **2017**, *2*, 2341.
[28] a) N. Jayaprakash, S. K. Das, L. A. Archer, *Chem. Commun.* **2011**, *47*, 12610; b) H. Li, H. Yang, Z. Sun, Y. Shi, H.-M. Cheng, F. Li, *Nano Energy* **2019**, *56*, 100; c) S. Wang, Z. Yu, J. Tu, J. Wang, D. Tian, Y. Liu, S. Jiao, *Adv. Energy Mater.* **2016**, *6*, 1600137; d) L. Geng, G. Lv, X. Xing, J. Guo, *Chem. Mater.* **2015**, *27*, 4926; e) X. Zhang, G. Zhang, S. Wang, S. Li, S. Jiao, *J. Mater. Chem. A* **2018**, *6*, 3084; f) S. Wang, S. Jiao, J. Wang, H. S. Chen, D. Tian, H. Lei, D. N. Fang, *ACS Nano* **2017**, *11*, 469; g) A. VahidMohammadi, A. Hadjikhani, S. Shahbazmohamadi, M. Beidaghi, *ACS Nano* **2017**, *11*, 11135; h) Z. Yu, Z. Kang, Z. Hu, J. Lu, Z. Zhou, S. Jiao, *Chem. Commun.* **2016**, *52*, 10427.
[29] K. V. Kravchyk, M. V. Kovalenko, *Adv. Energy Mater.* **2020**, *10*, 2002151.

Manuscript received: March 25, 2024
Accepted manuscript online: April 25, 2024
Version of record online: June 7, 2024